NANO LETTERS

Letter

Cite This: Nano Lett. 2018, 18, 7141−7145

pubs.acs.org/NanoLett

Single-Shot Readout of Hole Spins in Ge

Lada Vukušić,*,† Josip Kukučka,† Hannes Watzinger,† Joshua Michael Milem,† Friedrich Schäffler,‡ and Georgios Katsaros†

†Institute of Science and Technology Austria, Am Campus 1, 3400 Klosterneuburg, Austria

‡Johannes Kepler University, Institute of Semiconductor and Solid State Physics, Altenbergerstrasse 69, 4040 Linz, Austria

Supporting Information

ABSTRACT: The strong atomistic spin−orbit coupling of holes makes single-shot spin readout measurements difficult because it reduces the spin lifetimes. By integrating the charge sensor into a high bandwidth radio frequency reflectometry setup, we were able to demonstrate single-shot readout of a germanium quantum dot hole spin and measure the spin lifetime. Hole spin relaxation times of about 90 μs at 500 mT are reported, with a total readout visibility of about 70%. By analyzing separately the spin-to-charge conversion and charge readout fidelities, we have obtained insight into the processes limiting the visibilities of hole spins. The analyses suggest that high hole visibilities are feasible at realistic experimental conditions, underlying the potential of hole spins for the realization of viable qubit devices.

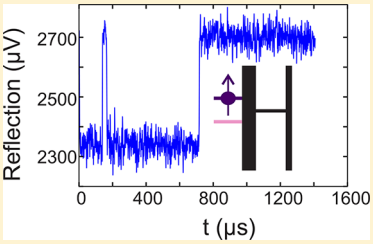

KEYWORDS: *Germanium, quantum dot, spin qubits, single-shot measurement, reflectometry*

Spin-based qubit systems have been in the focus of intense research in the past 15 years,[1,2] showing continuous improvement in the coherence times[3] and quality factor, the ratio between the qubit coherence and manipulation time.[4] One of the requirements for the realization of any type of qubit is a readout mechanism with high fidelity.[5] For spin 1/2 qubits and in single quantum dot devices this is realized optically by means of luminescence measurements[6] and electrically by spin to charge conversion. The latter was introduced in 2004 for electrons in GaAs.[7] A few years later, a similar scheme was used in order to measure the spin relaxation times for electrons in Si.[8,9] However, so far there has been no demonstration of single-shot hole spin readout despite the fact that holes are becoming more and more attractive as viable qubits[10−12] and have shown promising spin relaxation times.[13−15]

Here we study hole quantum dots (QDs) formed in Ge hut wires (HWs)[16] and we demonstrate for the first time single-shot hole spin readout. Due to the strong spin−orbit coupling,[17−20] which in general leads to shorter relaxation times,[1] we integrated the charge sensor into a radio frequency reflectometry setup.[21] Such a setup allows high bandwidths and the extraction of hole spin relaxation times, which were measured to be about 90 μs at 500 mT.

HWs are an appealing platform for building quantum devices with rich physics and technological potential. The confined hole wave function is almost of purely heavy-hole character,[22] which can lead to long spin coherence times.[23] Furthermore, they are monolithically grown on Si[16] without the use of any catalyst, making them fully compatible with CMOS technology. In addition, as self-assembled nanostructures can be grown on prepatterned Si substrates,[24,25] one can envision the growth of HWs at predefined positions.

The device used in this study consists of a QD formed at the end of a Ge HW and a charge sensor capacitively and tunnel coupled to it, which is used both as a hole reservoir and for the spin readout.[26] The charge sensor is a single hole transistor (SHT), formed in a HW that grows perpendicular to that hosting the spin qubit (Figure 1a). Whenever a hole tunnels from the QD to the charge sensor, a break in the SHT Coulomb peak appears (Figure 1b). In the presence of an external magnetic field, such a single hole tunnelling event becomes spin selective. In order to detect it, the Zeeman splitting, $E_Z = g\mu_B B$ must be larger than the width of the Fermi distribution of the SHT states, where g denotes the g-factor, μ_B the Bohr magneton, and B the applied magnetic field.

For performing single-shot measurements with high bandwidth, we used a reflectometry-based readout setup, where the SHT is part of the resonant circuit.[27−31] A radio frequency (RF) wave is sent toward the SHT and each change in its impedance manifests as a change in the amplitude of the reflected wave. All measurements were performed in a dilution refrigerator with a base temperature of ≈15 mK.

For the spin readout measurement we use the already well established three-stage pulsing sequence (Figure 2a) implemented by Elzerman et al.[7] to do spin-to-charge conversion. In a first stage (*load*), a hole with an unknown spin is loaded from the sensor into the dot. In a second stage (*read*), the electrochemical potentials of the QD for spin-up ($\mu_\uparrow$) and spin-down ($\mu_\downarrow$) are brought in a configuration where $\mu_\uparrow$ is above and $\mu_\downarrow$ below the electrochemical potential of the SHT (μ_{SHT}). With the last pulse (*empty*), the loaded hole tunnels

Received: August 7, 2018
Revised: October 2, 2018
Published: October 25, 2018

DOI: 10.1021/acs.nanolett.8b03217
Nano Lett. 2018, 18, 7141−7145

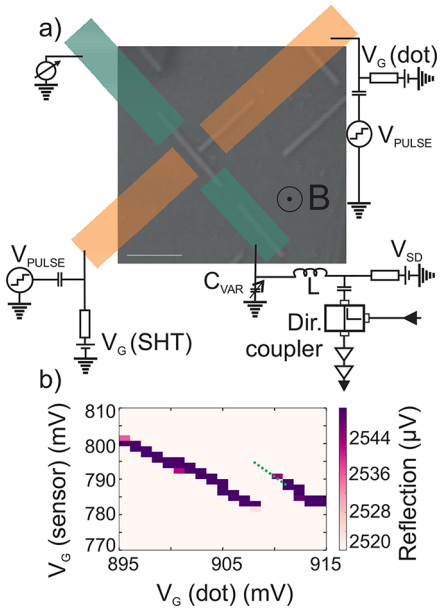

Figure 1. Spin readout device and schematics. (a) Schematic of a device similar to the one used for the spin readout with the scanning electron micrograph of the HWs in the background. Source and drain electrodes are shown in green; gates, in orange. The scale bar is 200 nm. (b) Zoom-in of a stability diagram obtained by sweeping the gate of the QD versus the gate of the charge sensor, at a magnetic field of 1100 mT. The pulsing sequence was applied along the upper part of the Coulomb peak break (green dashed line).

out of the QD. The charge sensor, SHT, shows a maximum (minimum) reflection amplitude (RA) when the QD is empty (loaded) (Figure 2b). In the read phase, one distinguishes between two cases, depending on whether a spin-up or spin-down hole has been loaded. In case a spin-down hole is loaded, the SHT RA stays at its minimum during the read stage. However, when a spin-up hole is loaded, it can tunnel out of the QD. As a consequence, the SHT RA obtains its maximum value; then it switches back to the minimum value when the QD gets refilled with a spin-down hole.

For determining, in the first place, the correct position of the read level for which spin dependent tunnelling is occurring, a similar three-stage sequence was applied (Figure 2c), with the difference that the amplitude of the read stage was varied. Averaging about 200 single-shot measurements reveals the spin signature (Figure 2d) as a purple tail at the beginning of the read phase between roughly −3 and −2 mV (black double arrow in Figure 2d). Different RA responses of the SHT are observed depending on the position of the read level, starting from too low (Figure 2e) to too high (Figure 2i). The green line in Figure 2d is positioned such that $\mu_\downarrow < \mu_{SHT} < \mu_\uparrow$. Two single-shot measurements taken at the position of the green line are shown in Figure 2f,g. Figure 2f corresponds to a loaded spin-up hole, while Figure 2g to a spin-down hole. For the neighboring break of the same Coulomb peak we do not see the spin signature, as this method works only when the QD has an even number of holes before the load stage. We note that in our measurements we could not see the existence of discrete energy levels in the SHT.

Once the correct position of the read level was determined, the sequence for spin readout was applied (Figure 3b, inset). In order to extract the hole spin relaxation time, the duration of the first, load stage of the pulse, is varied, while the durations of the read and empty stages are kept constant. The probability of observing a spin-up hole decreases exponentially with the

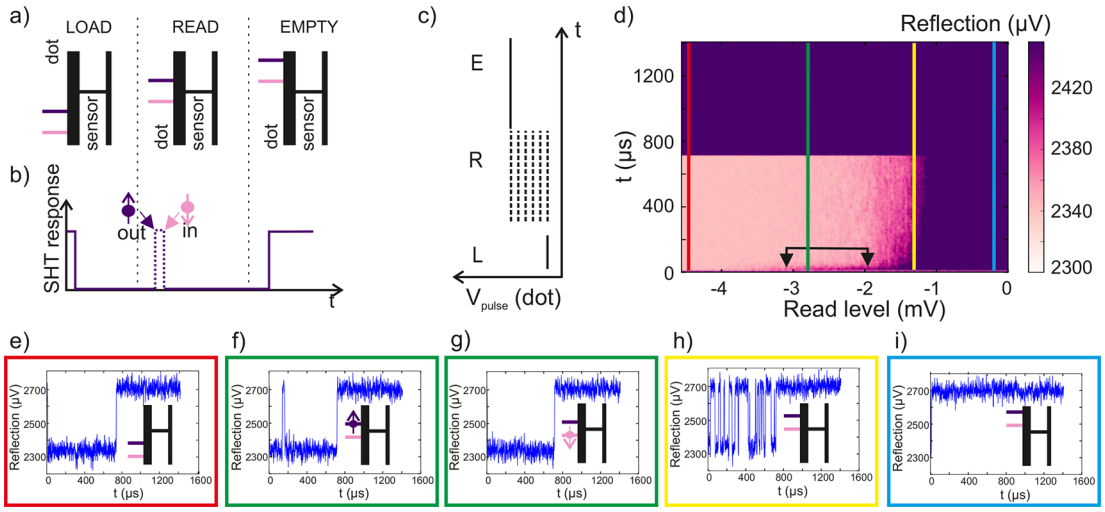

Figure 2. Single-shot spin readout and calibration of the read level. (a) Schematics showing the electrochemical potentials of the QD and the charge sensor during different stages of the pulsing sequence used for the single-shot spin readout. The lower electrochemical potential corresponds to a spin-down state. For simplicity throughout the manuscript the electron convention is used in the diagrams showing the alignment of the electrochemical potentials. (b) Expected response of the SHT when the sequence is applied along the upper part of the Coulomb peak break and a spin-up hole is loaded. (c) Three-stage pulsing sequence. The duration of the load stage is 8 μs and that of the read and empty stages 700 μs. (d) RA averaged over 197 single-shot traces as a function of the voltage applied on the QD gate during the read stage, taken at the magnetic field B = 1100 mT, with a detection bandwidth of 200 kHz. The double black arrow indicates the region where we see the spin signature. (e)−(i) Examples of single-shot traces. The schematics in the insets elucidate the alignment of the electrochemical potentials at the positions indicated by vertical lines in (d). (e) The read level is set too low: $\mu_\uparrow, \mu_\downarrow < \mu_{SHT}$, no hole can leave the QD during the read stage. (f) Correct position of the read level: $\mu_\downarrow < \mu_{SHT} < \mu_\uparrow$. Single-shot trace for the case of loading a spin-up hole. (g) Correct position of the read level: $\mu_\downarrow < \mu_{SHT} < \mu_\uparrow$. Single-shot trace for the case of loading a spin-down hole. (h) $\mu_\downarrow \approx \mu_{SHT}$. Random telegraph signal showing the continuous exchange of holes between the QD and the SHT. (i) The read level is set too high: $\mu_\uparrow, \mu_\downarrow > \mu_{SHT}$: the hole can always tunnel out during the read stage.

DOI: 10.1021/acs.nanolett.8b03217
Nano Lett. 2018, 18, 7141−7145

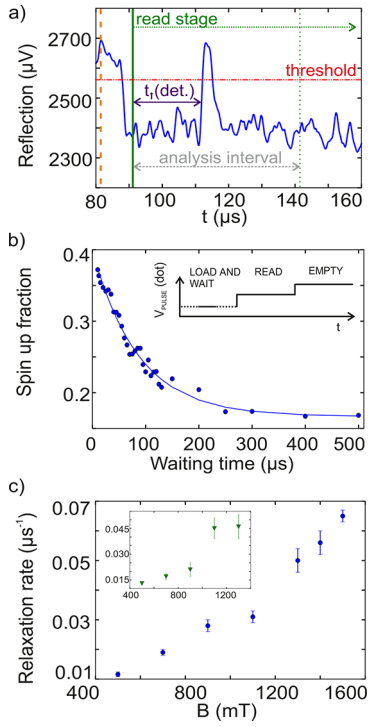

Figure 3. Spin relaxation rate. (a) Example of a single-shot trace for a loading time of 10 μs and for a magnetic field of 500 mT. The beginning of the load stage is labeled with the vertical dashed orange line and the moment when the levels of the dot are pulsed to the read stage with the vertical solid green line. The horizontal dot-dashed red line indicates the threshold above which a tunnelling event is considered to have taken place. All single-shot analysis was performed for an interval of 50 μs (gray dashed double arrow), as after the 50 μs and for tunnelling times of about 10 μs, the number of counts for spin-up tunnelling-out events is less than 1%. (b) Exponential decay of the spin-up fraction versus the waiting time for B = 500 mT. The three-stage pulsing sequence for measuring the spin relaxation time is shown in the inset. The duration of both the read and the empty stage is 700 μs and the duration of the load stage was varied from 10 to 500 μs. (c) Plot showing the spin relaxation rate vs magnetic field. The results for a second measured Coulomb peak break are shown in the inset. For the first break, the QD confines about 10−20 holes, while the second break corresponds to approximately 10 holes less. Despite this difference in the number of holes, the spin relaxation times and the magnetic field behavior are very similar.

waiting time. From the exponential decay, we extract a hole spin relaxation time T_1 of 86 ± 6 μs for an out-of-plane magnetic field of 500 mT (Figure 3b). As expected, the spin relaxation rate T_1^{-1} increases when increasing the magnetic field B (Figure 3c). We note that the values extracted from the single-shot measurements are in agreement with those extracted by integrating the averaged RA (see the Supporting Information).

The magnetic field dependence of T_1^{-1} does not follow a B^5 curve (Figure 3c), which is typically, but not always, observed for electrons in GaAs and Si.[1,8,9,32,33] For holes, the Bir−Pikus Hamiltonian, which describes the strain in the valence band, needs to be considered.[34] As it contains strain tensor elements and the spin operators,[19] it leads to a hole-phonon Hamiltonian that depends on both the spin and the phonons. This is different from the conduction band where the electron−phonon interaction does not depend on the spin. When the Bir−Pikus Hamiltonian was taken into account, a $B^{7/2}$ hole spin relaxation rate dependence was predicted for Ge/Si core/shell nanowires.[35] However, the experimental data reveal a $B^{1.5}$ for the first break and a $B^{1.4}$ for the second break dependence of the spin relaxation rate (see the Supporting Information) which deviates from what was predicted by theory for cylindrical nanowires. However, the theoretical predictions have been made for low energetic hole states. As we could not reach the last hole, we cannot be certain that we are in the same regime. In addition, the hole spin relaxation rates strongly depend on parameters as confinement and strain;[36,37] thus such a deviation is not a surprise.

To estimate the accuracy of the single-shot spin readout measurements, we followed a hybrid approach based on the methods introduced by Elzerman et al.[7] and Morello et al.[8] This approach allowed us to get insight in the limitations of hole spins as potential qubits. Initially, we extracted the spin-to-charge conversion fidelities. For each threshold used in the single-shot analysis, we extracted two parameters, α and β. Both correspond to a wrong assignment of the spin states. The parameter α gives the probability that the SHT signal exceeds the threshold even in the case of loading a spin-down hole and can be extracted from the saturation value of the spin-up fraction for very long waiting times (Figure 3b). The parameter β corresponds to the probability that a spin-up hole relaxes before it tunnels out. It is equal to $1/(1 + T_1\Gamma_\uparrow)$, where $\Gamma_\uparrow$ is the spin-up tunnel rate. From the fit to the histogram representing the detection times of the spin-up hole ($t_\uparrow$(det) in Figure 3a), one can extract the decay rate equal to ($\Gamma_\uparrow + T_1^{-1}$), which then allows the extraction of $\Gamma_\uparrow$ (see the Supporting Information). Due to the large setup bandwidth, β is largely threshold insensitive, as shown in Figure 4a for 500 mT. The spin-to-charge conversion fidelity for the spin-down hole ($1 - \alpha$) is 0.833 ± 0.005 while for the spin-up hole ($1 - \beta$) it is 0.907 ± 0.007, giving a maximum spin-to-charge conversion visibility ($1 - \alpha - \beta$) of 0.740 ± 0.009 for the normalized threshold of 0.7 (Figure 4a).

In order to get a better understanding of the the factors limiting the spin-to-charge conversion fidelities for holes, the dependence of α and β on the magnetic field was investigated (Figure 4b). While α tends to decrease for larger magnetic fields, β shows the opposite behavior. This leads to a maximum total spin-to-charge conversion visibility of 0.81 ± 0.01 at 700 mT. α implies mainly a failure of the spin-down hole to remain in the QD. The tunnel out time of the spin-down state and thus $1 - \alpha$ depends on the ratio of the magnetic field and the effective hole temperature (EHT).[9] One solution for increasing $1 - \alpha$ is to increase the magnetic field. However, larger magnetic fields imply short spin relaxation times and large qubit operation frequencies. The optimal solution is to keep the magnetic field at low values and decrease the effective hole temperature. Since the reported experiment was performed at an EHT of about 300−400 mK (see the Supporting Information), fidelities $1 - \alpha$ higher than 0.95 should be feasible at magnetic fields of about 200 mT for an EHT of 100 mK. We now turn our attention to β. As $\Gamma_\uparrow$ is rather insensitive to the magnetic field (see the Supporting Information), the increase of β originates from the drastically reduced spin relaxation times. Taking into account the $B^{3/2}$ dependence of the spin relaxation rate, relaxation times exceeding 0.3 ms should be feasible at 200 mT. This is in line with the values reported for core−shell wires at low magnetic fields.[13] Such longer spin relaxation times will allow $1 - \beta$ to exceed 0.95. From the above discussion it becomes clear that, regarding the

DOI: 10.1021/acs.nanolett.8b03217
Nano Lett. 2018, 18, 7141−7145

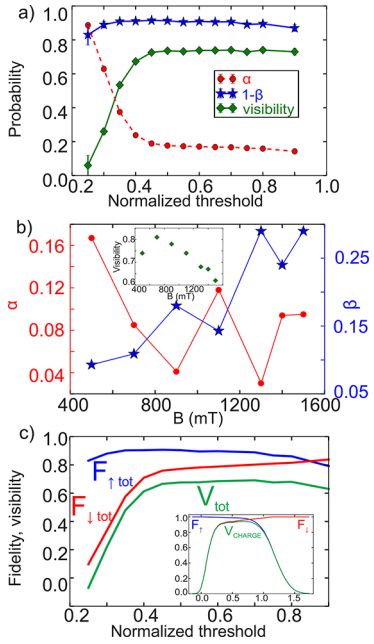

Figure 4. Measurement fidelity. (a) Dependence of α, $1 - \beta$, and the visibility on the normalized threshold, at $B = 500$ mT. Threshold = 1 corresponds to the average maximum SHT RA, and threshold = 0, to the average minimum SHT RA. (b) Magnetic field dependence of α (red dots) and β (blue stars), extracted for the threshold that gives the maximum visibility. The inset shows the dependence of the spin-to-charge visibility vs B. (c) Plot showing the total readout spin-down ($F_{\downarrow tot} = (1 - \alpha)*F_{\downarrow}$, red), spin-up ($F_{\uparrow tot} = (1 - \beta)*F_{\uparrow}$, blue) fidelity and the total readout visibility ($F_{\downarrow tot} + F_{\uparrow tot} - 1$, green). The inset shows the spin-down ($F_{\downarrow}$, red) and spin-up ($F_{\uparrow}$, blue) charge readout fidelities, as well as the charge readout visibility (green). The normalized threshold can exceed 1.0 as there are RA values exceeding the average maximum value.

spin-to-charge conversion fidelity, the main difference of hole spins compared to electron spins lies in β. While α for electron spins is as well limited by the magnetic field value,[9] this is not the case for β. For electron spins the spin relaxation time is in the order of seconds even at fields exceeding 1 T,[8,9] which in combination with the short tunnelling times makes β rather insensitive to the value of the magnetic field.

We now move to the charge readout fidelity. For this we performed a simulation following the procedure introduced by Morello et al.[8] (see the Supporting Information). Spin-down and spin-up fidelities of 0.962 and 0.980 were obtained (Figure 4c, inset). These fidelities are as high as those reported for electron spins because, for the charge readout fidelities, it is the measurement bandwidth that determines the extracted values. Finally, in order to obtain the total spin-up and spin-down fidelities and visibility of the single-shot measurements, the spin-to-charge conversion and charge readout fidelities were multiplied (Figure 4c). The total spin-down (up) hole fidelity is given by 0.801 ± 0.005 (0.889 ± 0.007) and the total visibility of the single shot readout measurements is 0.691 ± 0.008. These values correspond to the normalized threshold of 0.7. When the same analysis was repeated for 700 mT, a total visibility of 0.752 ± 0.009 was obtained (see the Supporting Information).

In summary, as the interest in hole spin qubits[10,12] has been continuously increasing over the past few years,[38−42] the demonstration of hole spin readout in single QD devices is an important first step toward more complex geometries.[43−45] The reported spin-to-charge conversion and charge readout out fidelities suggest that hole devices operated at low magnetic fields can lead to qubits with very high spin readout fidelities. The reported results, together with the CMOS compatibility, the possibility of isotopical purification, and the strong spin−orbit coupling, suggest Ge as a promising material system for moving toward long-range coupling and spin entanglement.[46,47]

■ ASSOCIATED CONTENT

Supporting Information

The Supporting Information is available free of charge on the ACS Publications website at DOI: 10.1021/acs.nanolett.8b03217.

Growth, fabrication, and setup details, logarithmic plots of relaxation rate vs magnetic field, averaged spin relaxation measurements, deterministic loading of the spin-down state and spin relaxation time measurements, lever arm and effective hole temperature measurements, charge readout fidelity, and measurement fidelity for higher magnetic field. (PDF)

■ AUTHOR INFORMATION

Corresponding Author

*L. Vukušić. E-mail: lada.vukusic@ist.ac.at. Phone: +43 2243 9000 721204.

ORCID

Lada Vukušić: 0000-0003-2424-8636

Notes

The authors declare no competing financial interest.

■ ACKNOWLEDGMENTS

We thank C. Kloeffel, A. Laucht, D. Loss, and M. Veldhorst for helpful discussions. The work was supported by the ERC Starting Grant no. 335497, the FWF-Y 715-N30 project, and the Austrian Ministry of Science through the HRSM call 2016. This research was supported by the Scientic Service Units of IST Austria through resources provided by the MIBA Machine Shop and the Nanofabrication Facility.

■ REFERENCES

(1) Hanson, R.; Kouwenhoven, L. P.; Petta, J. R.; Tarucha, S.; Vandersypen, L. M. K. *Rev. Mod. Phys.* **2007**, *79*, 1217−1265.

(2) Zwanenburg, A.; Dzurak, A. S.; Morello, A.; Simmons, M. Y.; Hollenberg, L. C. L.; Klimeck, G.; Rogge, S.; Coppersmith, S. N.; Eriksson, M. A. *Rev. Mod. Phys.* **2013**, *85*, 961−1019.

(3) Muhonen, J. T.; Dehollain, J. P.; Laucht, A.; Hudson, F. E.; Kalra, R.; Sekiguchi, T.; Itoh, K. M.; Jamieson, D. N.; McCallum, J. C.; Dzurak, A. S.; Morello, A. *Nat. Nanotechnol.* **2014**, *9*, 986−991.

(4) Yoneda, J.; Takeda, K.; Otsuka, T.; Nakajima, T.; Delbecq, M. R.; Allison, G.; Honda, T.; Kodera, T.; Oda, S.; Hoshi, Y.; Usami, N.; Itoh, K. M.; Tarucha, S. *Nat. Nanotechnol.* **2018**, *13*, 102−106.

(5) DiVincenzo, D. P. *Fortschr. Phys.* **2000**, *48*, 771−783.

(6) Warburton, R. J. *Nat. Mater.* **2013**, *12*, 483−493.

(7) Elzerman, J. M.; Hanson, R.; van Beveren, L. H. W.; Witkamp, B.; Vandersypen, L. M. K.; Kouwenhoven, L. P. *Nature* **2004**, *430*, 431−435.

(8) Morello, A.; Pla, J. J.; Zwanenburg, A.; Chan, K. W.; Tan, K. Y.; Huebl, H.; Möttönen, M.; Nugroho, C. D.; Yang, C.; van Donkelaar, J. A.; Alves, A. D. C.; Jamieson, D. N.; Escott, C. C.; Hollenberg, L. C. L.; Clark, R. G.; Dzurak, A. S. *Nature* **2010**, *467*, 687−691.

(9) Büch, H.; Mahapatra, S.; Rahman, R.; Morello, A.; Simmons, M. Y. *Nat. Commun.* **2013**, *4*, 2017.

DOI: 10.1021/acs.nanolett.8b03217
Nano Lett. 2018, 18, 7141−7145

(10) Maurand, R.; Jehl, X.; Kotekar-Patil, D.; Corna, A.; Bohuslavskyi, H.; Laviéville, R.; Hutin, L.; Barraud, S.; Vinet, M.; Sanquer, M.; De Franceschi, S. *Nat. Commun.* **2016**, *7*, 13575.
(11) Prechtel, J. H.; Kuhlmann, A. V.; Houel, J.; Ludwig, A.; Valentin, S. R.; Wieck, A. D.; Warburton, R. J. *Nat. Mater.* **2016**, *15*, 981−986.
(12) Watzinger, H.; Kukučka, J.; Vukušić, L.; Gao, F.; Wang, T.; Schäffler, F.; Zhang, J. J.; Katsaros, G. *Nat. Commun.* **2018**, *9*, 3902.
(13) Hu, Y.; Kuemmeth, F.; Lieber, C. M.; Marcus, C. M. *Nat. Nanotechnol.* **2012**, *7*, 47−50.
(14) Gerardot, B. D.; Brunner, D.; Dalgarno, P. A.; Öhberg, P.; Seidl, S.; Kroner, M.; Karrai, K.; Stoltz, N. G.; Petroff, P. M.; Warburton, R. J. *Nature* **2008**, *451*, 441−444.
(15) Heiss, D.; Schaeck, S.; Huebl, H.; Bichler, M.; Abstreiter, G.; Finley, J. J.; Bulaev, D. V.; Loss, D. *Phys. Rev. B: Condens. Matter Mater. Phys.* **2007**, *76*, 241306.
(16) Zhang, J. J.; Katsaros, G.; Montalenti, F.; Scopece, D.; Rezaev, R. O.; Mickel, C.; Rellinghaus, B.; Miglio, L.; De Franceschi, S.; Rastelli, A.; Schmidt, O. G. *Phys. Rev. Lett.* **2012**, *109*, 085502.
(17) Hao, X.-J.; Tu, T.; Cao, G.; Zhou, C.; Li, H.-O.; Guo, G.-C.; Fung, W. Y.; Ji, Z.; Guo, G.-P.; Lu, W. *Nano Lett.* **2010**, *10*, 2956−2960.
(18) Higginbotham, A. P.; Kuemmeth, F.; Larsen, T. W.; Fitzpatrick, M.; Yao, J.; Yan, H.; Lieber, C. M.; Marcus, C. M. *Phys. Rev. Lett.* **2014**, *112*, 216806.
(19) Kloeffel, C.; Rančić, M. J.; Loss, D. *Phys. Rev. B: Condens. Matter Mater. Phys.* **2018**, *97*, 235422.
(20) Marcellina, E.; Hamilton, A. R.; Winkler, R.; Culcer, D. *Phys. Rev. B: Condens. Matter Mater. Phys.* **2017**, *95*, 075305.
(21) Schoelkopf, R. J.; Wahlgren, P.; Kozhevnikov, A. A.; Delsing, P.; Prober, D. E. *Science* **1998**, *280*, 1238−1242.
(22) Watzinger, H.; Kloeffel, C.; Vukušić, L.; Rossel, M.; Sessi, V.; Kukučka, J.; Kirchschlager, R.; Lausecker, E.; Truhlar, A.; Glaser, M.; Rastelli, A.; Fuhrer, A.; Loss, D.; Katsaros, G. *Nano Lett.* **2016**, *16*, 6879−6885.
(23) Fischer, J.; Coish, W. A.; Bulaev, D. V.; Loss, D. *Phys. Rev. B: Condens. Matter Mater. Phys.* **2008**, *78*, 155329.
(24) Katsaros, G.; Tersoff, J.; Stoffel, M.; Rastelli, A.; P, A.-D.; Kar, G. S.; Costantini, G.; Schmidt, O. G.; Kern, K. *Phys. Rev. Lett.* **2008**, *101*, 096103.
(25) Zhang, J. J.; Stoffel, M.; Rastelli, A.; Schmidt, O. G.; Jovanović, V.; Nanver, L. K.; Bauer, G. *Appl. Phys. Lett.* **2007**, *91*, 173115.
(26) Vukušić, L.; Kukučka, J.; Watzinger, H.; Katsaros, G. *Nano Lett.* **2017**, *17*, 5706−5710.
(27) Reilly, D. J.; Marcus, C. M.; Hanson, M. P.; Gossard, A. C. *Appl. Phys. Lett.* **2007**, *91*, 162101.
(28) Jung, M.; Schroer, M. D.; Petterson, K. D.; Petta, J. R. *Appl. Phys. Lett.* **2012**, *100*, 253508.
(29) Frake, J. C.; Kano, S.; Ciccarelli, C.; Griffiths, J.; Sakamoto, M.; Teranishi, T.; Majima, Y.; Smith, C. G.; Buitelaar, M. R. *Sci. Rep.* **2015**, *5*, 10858.
(30) Ares, N.; Schupp, F. J.; Mavalankar, A.; Rogers, G.; Griffiths, J.; Jones, G. A. C.; Farrer, I.; Ritchie, D. A.; Smith, C. G.; Cottet, A.; Briggs, G. A. D.; Laird, E. A. *Phys. Rev. Appl.* **2016**, *5*, 034011.
(31) Hile, S. J.; House, M. G.; Peretz, E.; Verduijn, J.; Widmann, D.; Kobayashi, T.; Rogge, S.; Simmons, M. Y. *Appl. Phys. Lett.* **2015**, *107*, 093504.
(32) Yang, C. H.; Rossi, A.; Ruskov, R.; Lai, N. S.; Mohiyaddin, F. A.; Lee, S.; Tahan, C.; Klimeck, G.; Morello, A.; Dzurak, A. S. *Nat. Commun.* **2013**, *4*, 2069.
(33) Camenzind, L. C.; Yu, L.; Stano, P.; Zimmerman, J. D.; Gossard, A. C.; Loss, D.; Zumbühl, D. M. *Nat. Commun.* **2018**, *9*, 3454.
(34) Bir, G. L.; Pikus, G. E. *Symmetry and Strain-induced Effects in Semiconductors*; Wiley: New York, 1974.
(35) Maier, F.; Kloeffel, C.; Loss, D. *Phys. Rev. B: Condens. Matter Mater. Phys.* **2013**, *87*, 161305.
(36) Woods, L. M.; Reinecke, T. L.; Kotlyar, R. *Phys. Rev. B: Condens. Matter Mater. Phys.* **2004**, *69*, 125330.
(37) Lü, C.; Cheng, J. L.; Wu, M. W. *Phys. Rev. B: Condens. Matter Mater. Phys.* **2005**, *71*, 075308.
(38) Hendrickx, N. W.; Franke, D. P.; Sammak, A.; Kouwenhoven, M.; Sabbagh, D.; Yeoh, L.; Li, R.; Tagliaferri, M. L. V.; Virgilio, M.; Capellini, G.; Scappucci, G.; Veldhorst, M. *Nat. Commun.* **2018**, *9*, 2835.
(39) Brauns, M.; Ridderbos, J.; Li, A.; Bakkers, E. P. A. M.; van der Wiel, W. G.; Zwanenburg, F. A. *Phys. Rev. B: Condens. Matter Mater. Phys.* **2016**, *94*, 041411.
(40) Li, R.; Hudson, F. E.; Dzurak, A. S.; Hamilton, A. R. *Nano Lett.* **2015**, *15*, 7314−7318.
(41) Wang, D. Q.; Klochan, O.; Hung, J.-T.; Culcer, D.; Farrer, I.; Ritchie, D. A.; Hamilton, A. R. *Nano Lett.* **2016**, *16*, 7685−7689.
(42) Hung, J.-T.; Marcellina, E.; Wang, B.; Hamilton, A. R.; Culcer, D. *Phys. Rev. B: Condens. Matter Mater. Phys.* **2017**, *95*, 195316.
(43) Zajac, D. M.; Sigillito, A. J.; Russ, M.; Borjans, F.; Taylor, J. M.; Burkard, G.; Petta, J. R. *Science* **2018**, *359*, 439−442.
(44) Veldhorst, M.; Yang, C. H.; Hwang, J. C. C.; Huang, W.; Dehollain, J. P.; Muhonen, J. T.; Simmons, S.; Laucht, A.; Hudson, F. E.; Itoh, K. M.; Morello, A.; Dzurak, A. S. *Nature* **2015**, *526*, 410−414.
(45) Watson, T. F.; Philips, S. G. J.; Kawakami, E.; Ward, D. R.; Scarlino, P.; Veldhorst, M.; Savage, D. E.; Lagally, M. G.; Friesen, M.; Coppersmith, S. N.; Eriksson, M. A.; Vandersypen, L. M. K. *Nature* **2018**, *555*, 633.
(46) Nigg, S. E.; Fuhrer, A.; Loss, D. *Phys. Rev. Lett.* **2017**, *118*, 147701.
(47) Kloeffel, C.; Trif, M.; Stano, P.; Loss, D. *Phys. Rev. B: Condens. Matter Mater. Phys.* **2013**, *88*, 241405.

DOI: 10.1021/acs.nanolett.8b03217
Nano Lett. 2018, 18, 7141−7145